eLIFE
elifesciences.org

Figures and figure supplements

MOF-associated complexes ensure stem cell identity and *Xist* repression

Tomasz Chelmicki, et al.

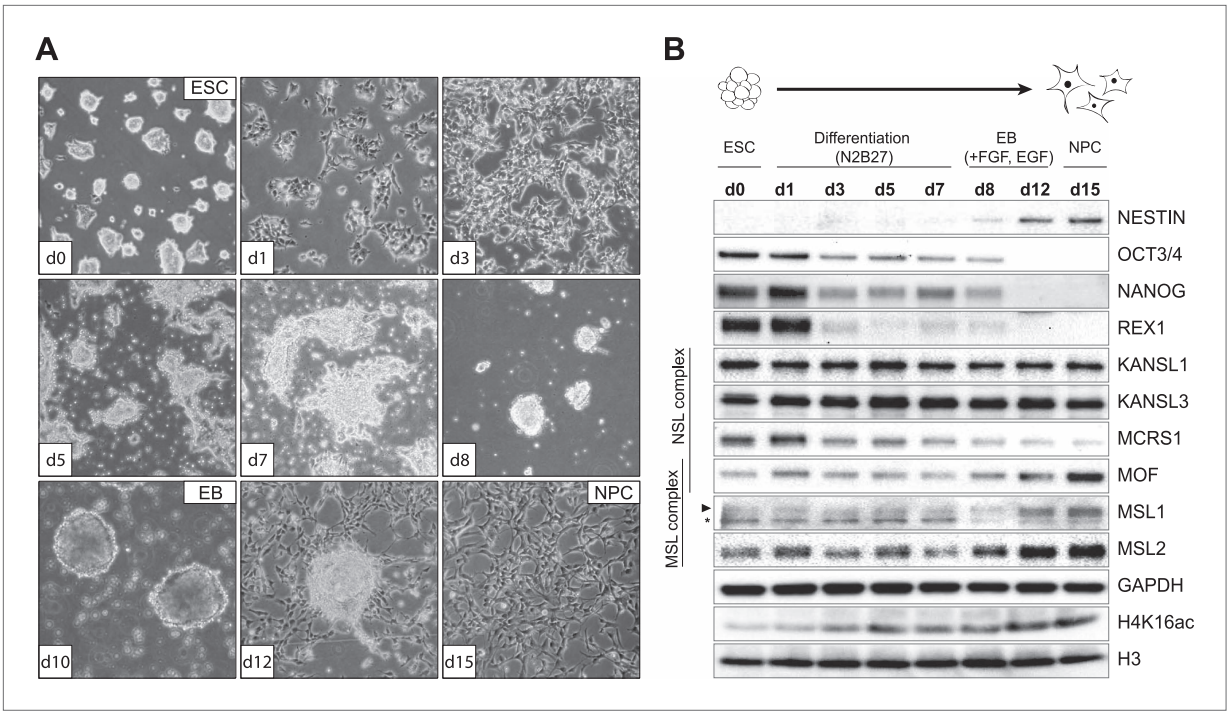

Figure 1. Distinct dynamics of MOF, MSL and NSL complexes during differentiation from ESCs to NPCs. (**A**) We monitored the cell morphology during differentiation of mouse embryonic stem cells into neuronal progenitor cells (NPC) via embryoid body formation (EB) with bright field microscopy. The day of differentiation is indicated in white boxes. (**B**) Western blot analysis for ESC to NPC differentiation. Stages of differentiation together with the day of differentiation (d0–d15) are indicated on top. GAPDH and histone 3 (H3) were used as loading controls. For expression analysis see ***Figure 1—figure supplement 1***.

DOI: 10.7554/eLife.02024.003

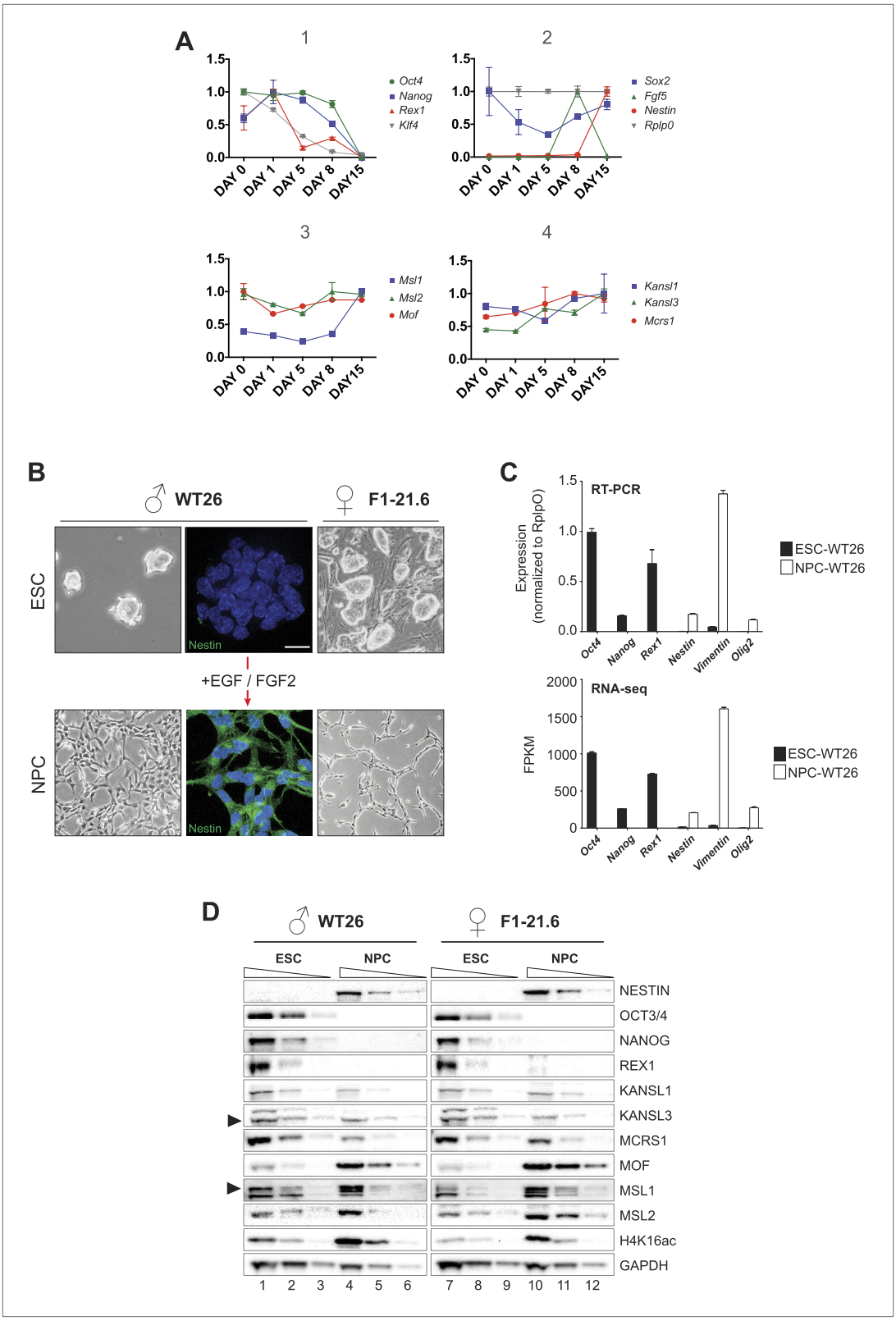

Figure 1—figure supplement 1. Monitoring RNA and protein levels in ESCs and NPCs.

DOI: 10.7554/eLife.02024.004

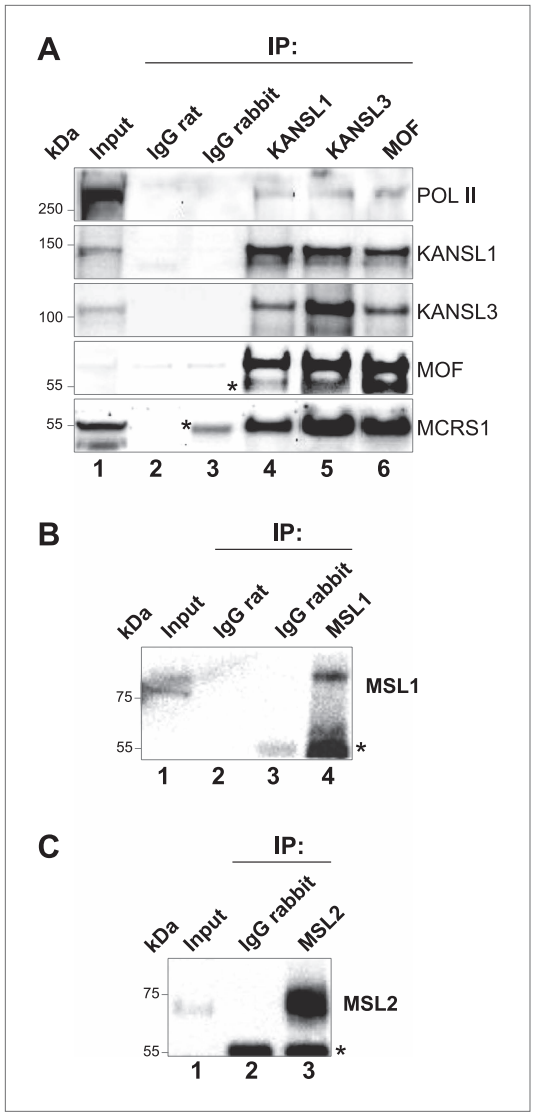

Figure 1—figure supplement 2. Verification of antibodies used in this study.
DOI: 10.7554/eLife.02024.005

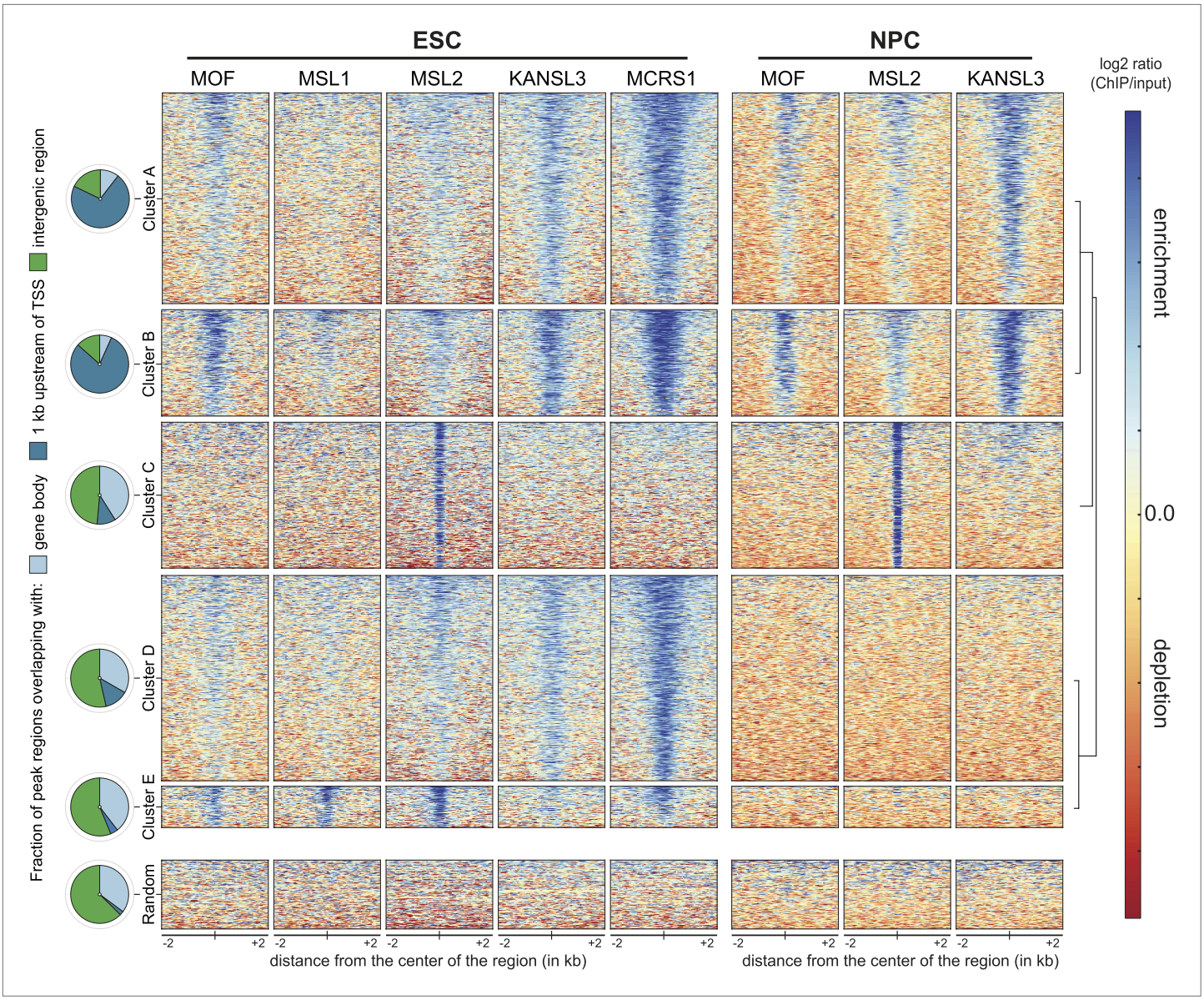

Figure 2. Distinct and shared binding sites of MOF and its complexes in mouse ESCs and NPCs. We applied unsupervised clustering on the union of peaks from all ChIP-seq samples and thereby identified five distinct groups of binding for MOF, MSL and NSL proteins in ESCs and NPCs. Shown here are the input-normalized ChIP signals for each cluster of peaks including a size-matched control set of random genomic regions. The order of the regions is the same for all columns. The pie charts on the left indicate the number of regions from each cluster that overlap with gene bodies, the region 1 kb upstream of genes' TSS or intergenic regions.

DOI: 10.7554/eLife.02024.006

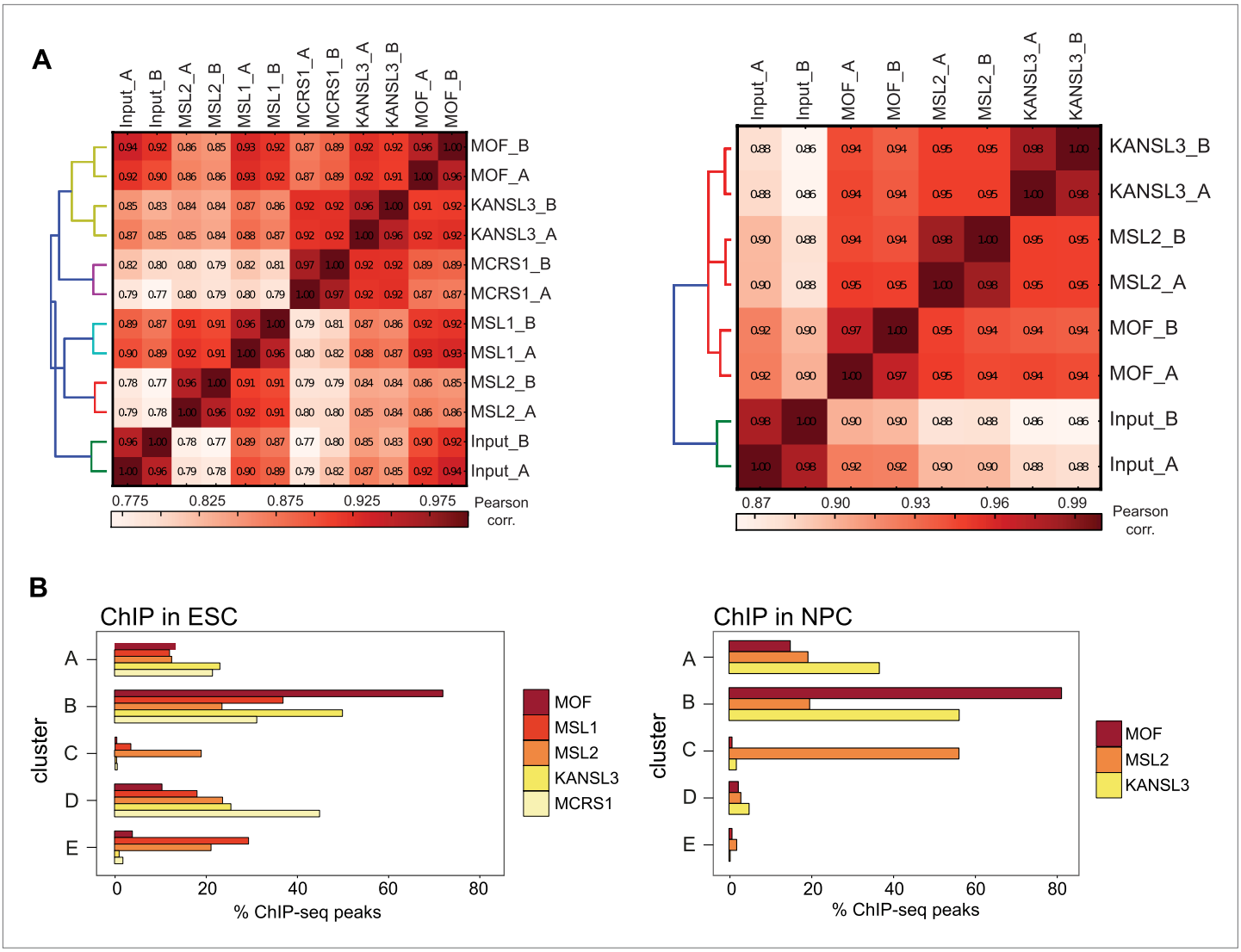

Figure 2—figure supplement 1. ChIP-seq quality measures.

DOI: 10.7554/eLife.02024.007

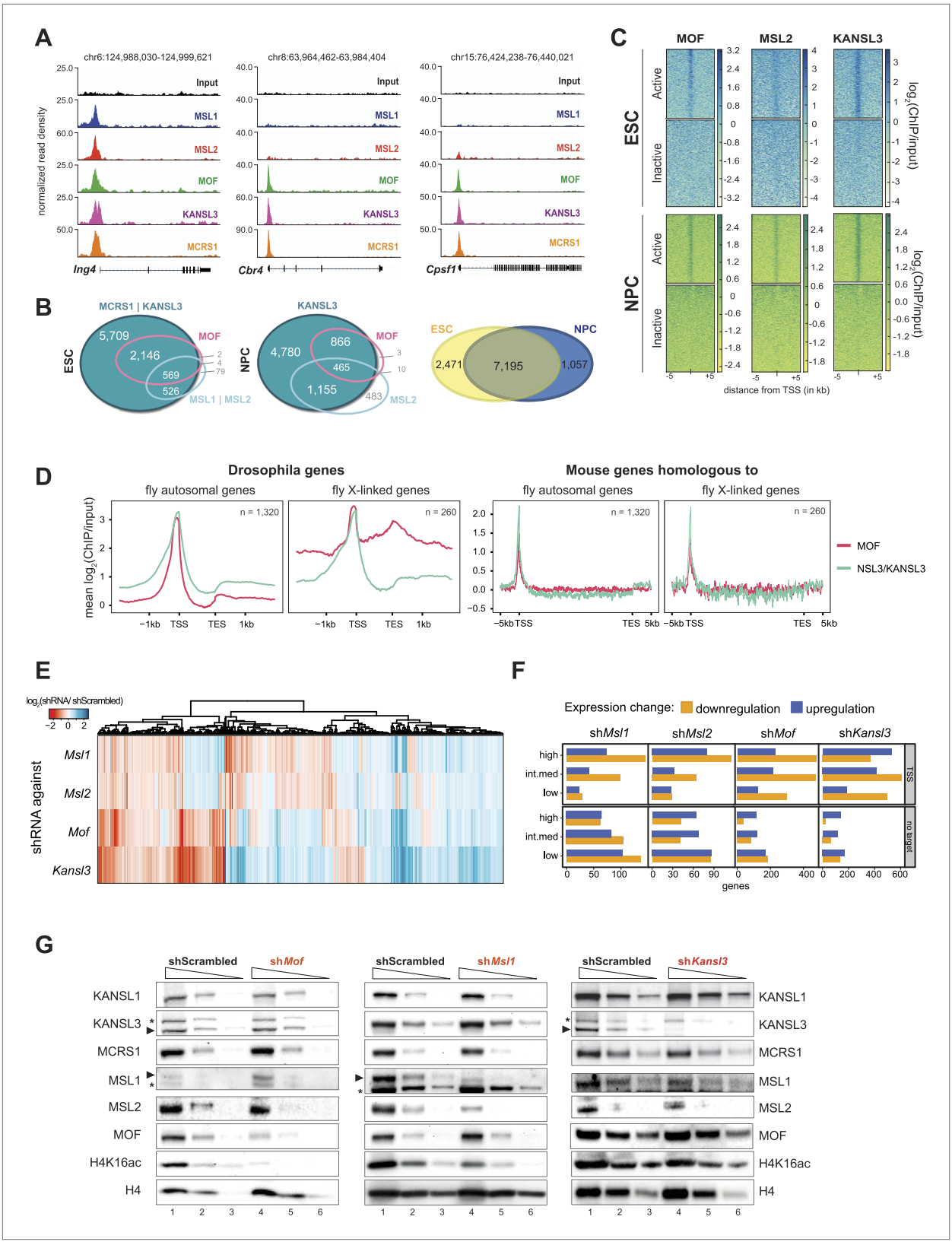

Figure 3. Both MOF-complexes bind to the TSS of broadly expressed genes in mouse ESCs and NPCs. (**A**) Genome browser snapshots of genes targeted by MSL and NSL complexes or by the NSL complex only. Signals were sequencing-depth-normalized and from ESCs. For ChIP-qPCR-based validation of the signals see ***Figure 3—figure supplement 4B***. (**B**) Venn diagrams of genes whose promoter regions (TSS ± 500 bp) overlapped with

Figure 3. Continued on next page

Figure 3. Continued

ChIP-seq peaks of NSL complex members (KANSL3 and/or MCRS1), MOF and MSL complex members (MSL1 and/or MSL2). The right-most panel depicts the overlap of genes bound by at least one factor in ESCs and NPCs. (**C**) The heatmaps display the input-normalized ChIP enrichments of MOF, MSL2 and KANSL3 around the TSS of genes that were active in ESCs as well as NPCs based on RNA-seq data that we generated for both cell types. (**D**) Summary plots of genes bound by the NSL complex in *D. melanogaster* for which mouse homologues were found. The input-normalized ChIP-seq signals around the TSS reveal markedly increased binding of MOF for male X-linked fly genes (left panels) that was not recapitulated in the mouse (right panels; ChIP-seq signals from ESCs). Fly genes were scaled to 1.2 kb and values were extracted from published data sets, mouse genes were scaled to 30 kb. (**E**) Heatmap depicting results of RNA-seq experiments from different shRNA-treated cells. The colors correspond to $\log_2$ fold changes (shRNA-treated cells/scrambled control) for genes whose expression was significantly affected in all knockdown conditions. Values were ordered using hierarchical clustering. (**F**) Bar plot of gene counts for different gene classes. We determined significantly up- and downregulated genes for each knockdown condition and binned them according to their expression strength in wild-type ESCs (high, intermediate, low). Then, for each gene, information about the TSS-targeting was extracted from the corresponding ChIP-seq sample. Non-target genes are neither bound at the promoter nor the gene body and were not predicted to be regulated via TSS-distal binding sites in any of the 5 ChIP-seq ESC samples. For details on the target classification see 'Materials and methods'. (**G**) Western blot analysis of MSL and NSL complex members and H4K16 acetylation in scrambled-, *Mof*-, *Msl1*-, and *Kansl3*-shRNA-treated male ESCs. Three concentrations (100%, 30%, 10%) of RIPA extract were loaded per sample. Asterisks mark the position of unspecific bands; triangles indicate the protein of interest.

DOI: 10.7554/eLife.02024.008

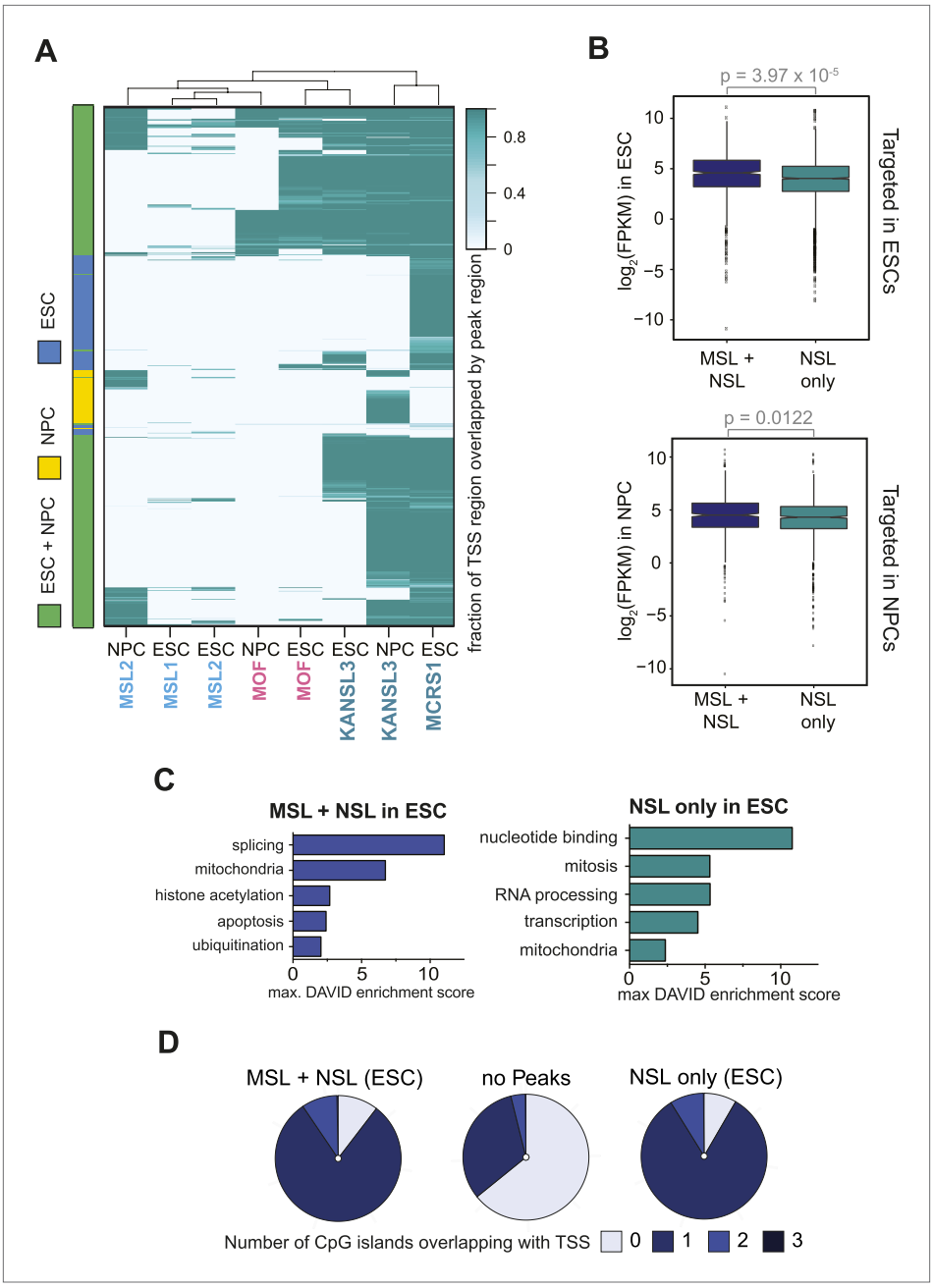

Figure 3—figure supplement 1. MSL and NSL complexes target promoters of broadly expressed genes in ESCs and NPCs.

DOI: 10.7554/eLife.02024.009

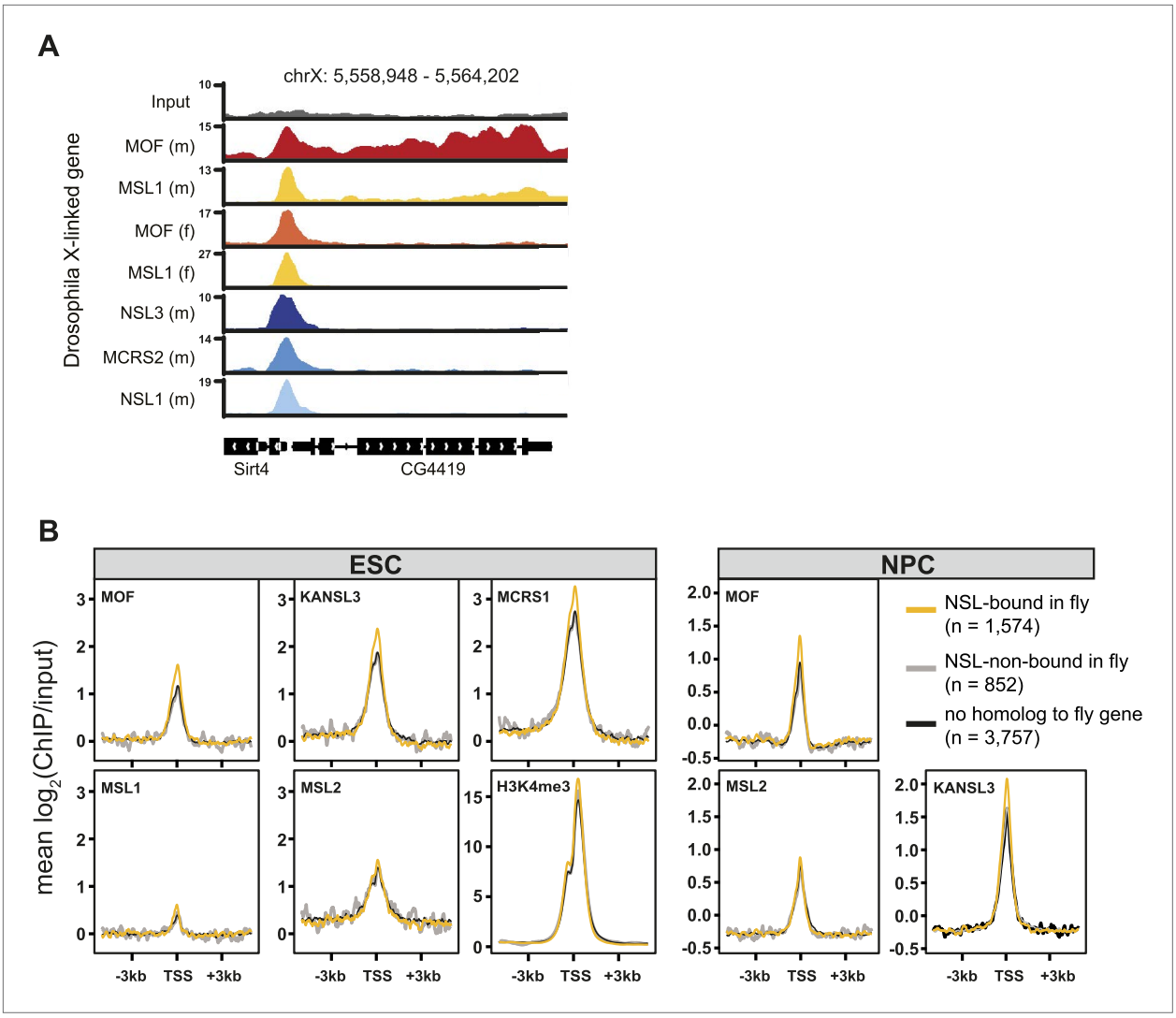

Figure 3—figure supplement 2. The NSL-, but not the MSL-binding mode of *D. melanogaster* is present in mammalian cells.
DOI: 10.7554/eLife.02024.010

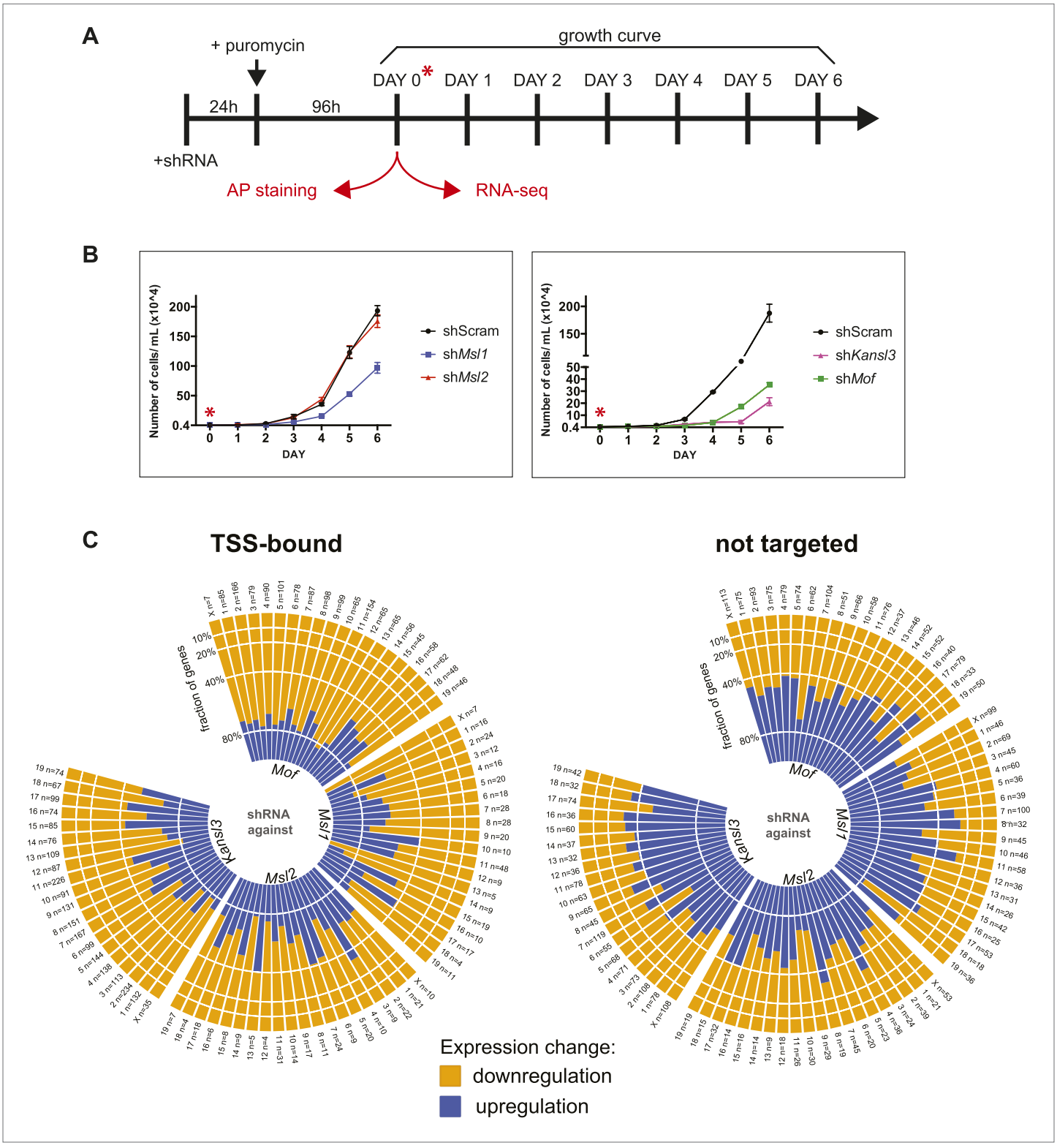

Figure 3—figure supplement 3. Effects of shRNA-mediated depletion of MOF, MSL1, MSL2 and KANSL3.
DOI: 10.7554/eLife.02024.011

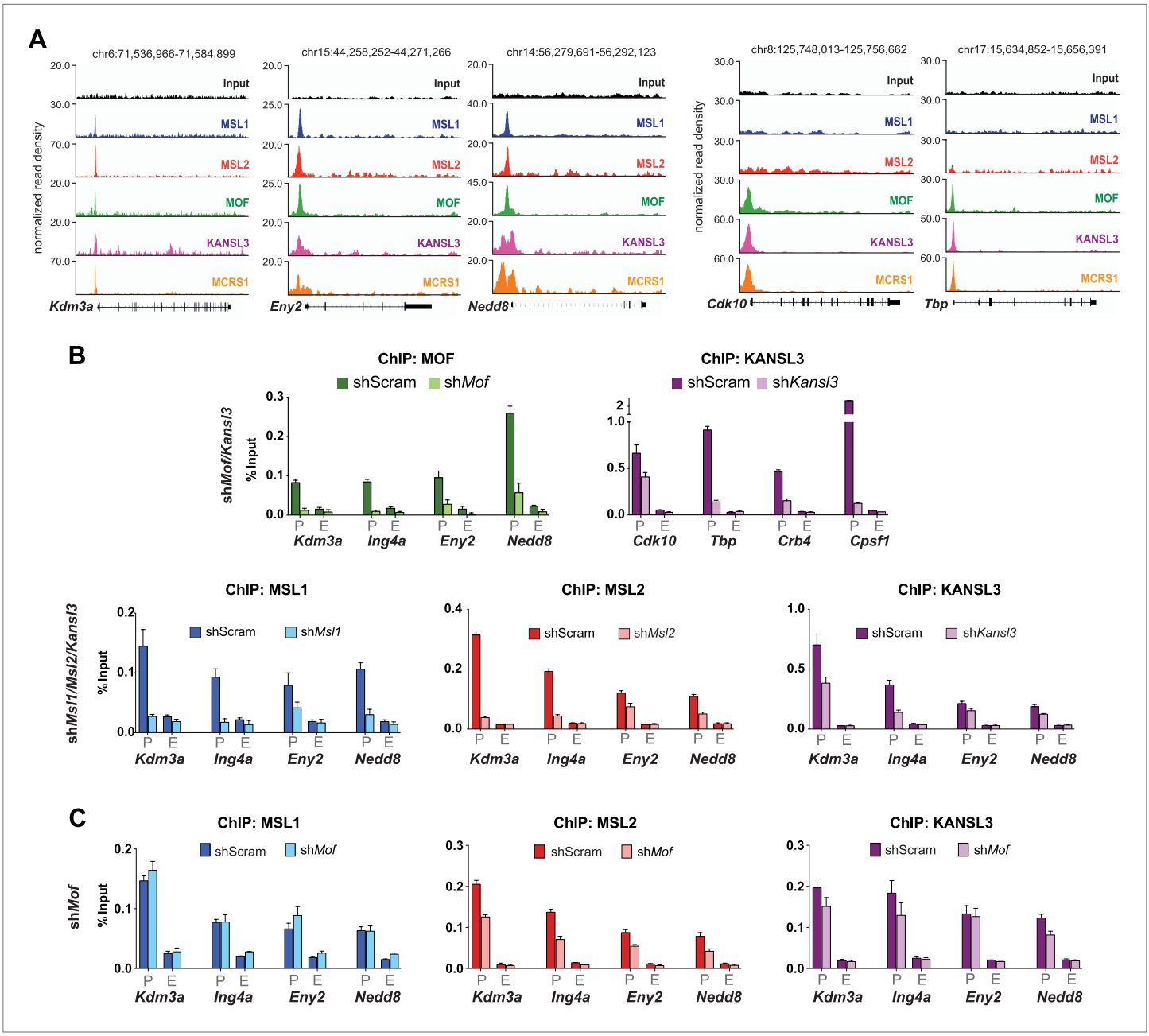

Figure 3—figure supplement 4. Assessment of ChIP signals around the TSSs of putative target genes as determined by ChIP-seq.
DOI: 10.7554/eLife.02024.012

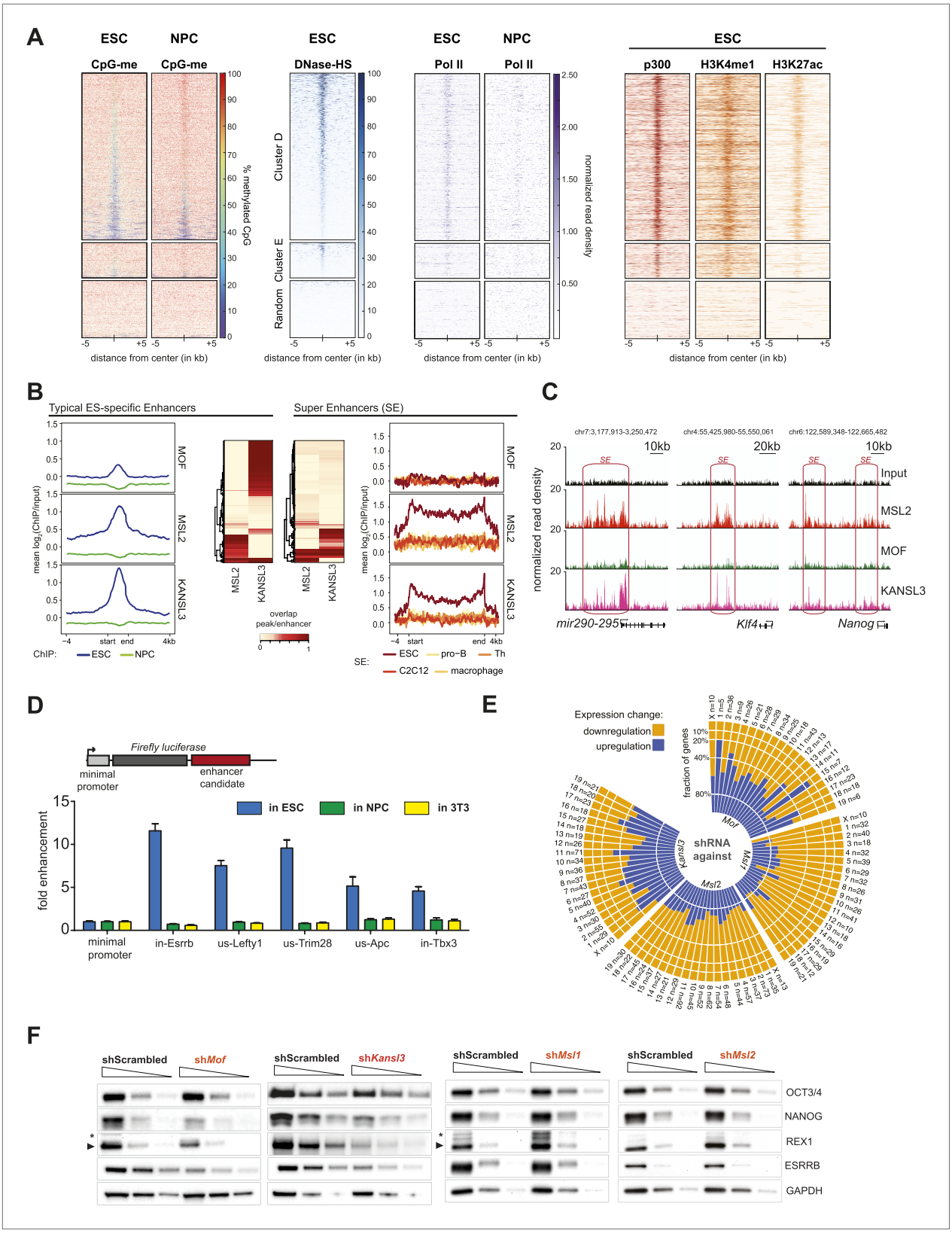

Figure 4. MSL and NSL complex members are enriched at regions with enhancer marks in ESCs. (**A**) Shown here are the fractions of methylated cytosines and ChIP-seq read densities of enhancer markers for regions of ESC-specific enrichments of our proteins of interest. We downloaded the different data from public repositories (see ***Supplementary file 3A*** for details) and calculated the values for the regions of the ESC-specific clusters **D** and **E** and

Figure 4. Continued on next page

Figure 4. Continued

random genomic loci. Most data sets used here were from mouse ESC except one RNA Polymerase II (Pol II) sample from NPC. All heatmaps were sorted according to the DNase hypersensitivity values except for CpG methylation heatmaps which were sorted according to their own values. (**B**) Summary plots of input-normalized ChIP-seq signals along typical (TE) and super enhancers (SE) (***Whyte et al., 2013***). Note that we show the ESC-specific TE only while on the right-hand side we show the signal for SE regions from several cell types. Enhancer regions were scaled to 30 kb (SE) and circa 700 bp (TE). The heatmaps between the summary plots depict how much of each enhancer region overlaps with ChIP-seq peaks of MSL2 or KANSL3. ESC = embryonic stem cells (n = 232), pro-B = progenitor B cells (n = 396), Th = T helper cells (n = 437), C2C12 = myotube cells (n = 536). (**C**) Exemplary genome browser snapshots of annotated super enhancers (SE, pink boxes) for three pluripotency factors displaying the sequencing-depth normalized ESC ChIP-seq signals of MSL2, MOF and KANSL3. See ***Figure 4—figure supplement 4C*** for additional examples. (**D**) Luciferase assays demonstrate the biological activity of regions bound by MOF-associated proteins in ESCs ('in' stands for intronic region, 'us' indicates that the cloned region is upstream of the gene). The firefly luciferase gene was cloned under a minimal promoter together with the putative enhancer region in ESCs, NPCs, and 3T3 cells. The graphs represent at least three independent experiments performed in technical triplicates; error bars represent SEM. (**E**) Bar plots depicting the fraction of significantly up- and downregulated genes per chromosome in the different shRNA-treated cells compared to shScrambled controls (total number of significantly affected genes per sample and chromosome labels are indicated). All genes counted here were classified as TSS-distal target genes in the respective ChIP-seq experiments. See 'Materials and methods' for details of the classifications. (**F**) Western blot analyses of the pluripotency factors in scrambled-, *Mof*-, *Kansl3*-, *Msl1*-, and *Msl2*-shRNA-treated male ESCs. For additional analyses in female ESCs see ***Figure 6C***. The respective dilution (100%, 30%, 10%) of loaded RIPA extract is indicated above each panel. Asterisks mark the position of unspecific bands; triangles indicate the protein of interest. GAPDH was used as the loading control. For antibodies see 'Materials and methods'.

DOI: 10.7554/eLife.02024.013

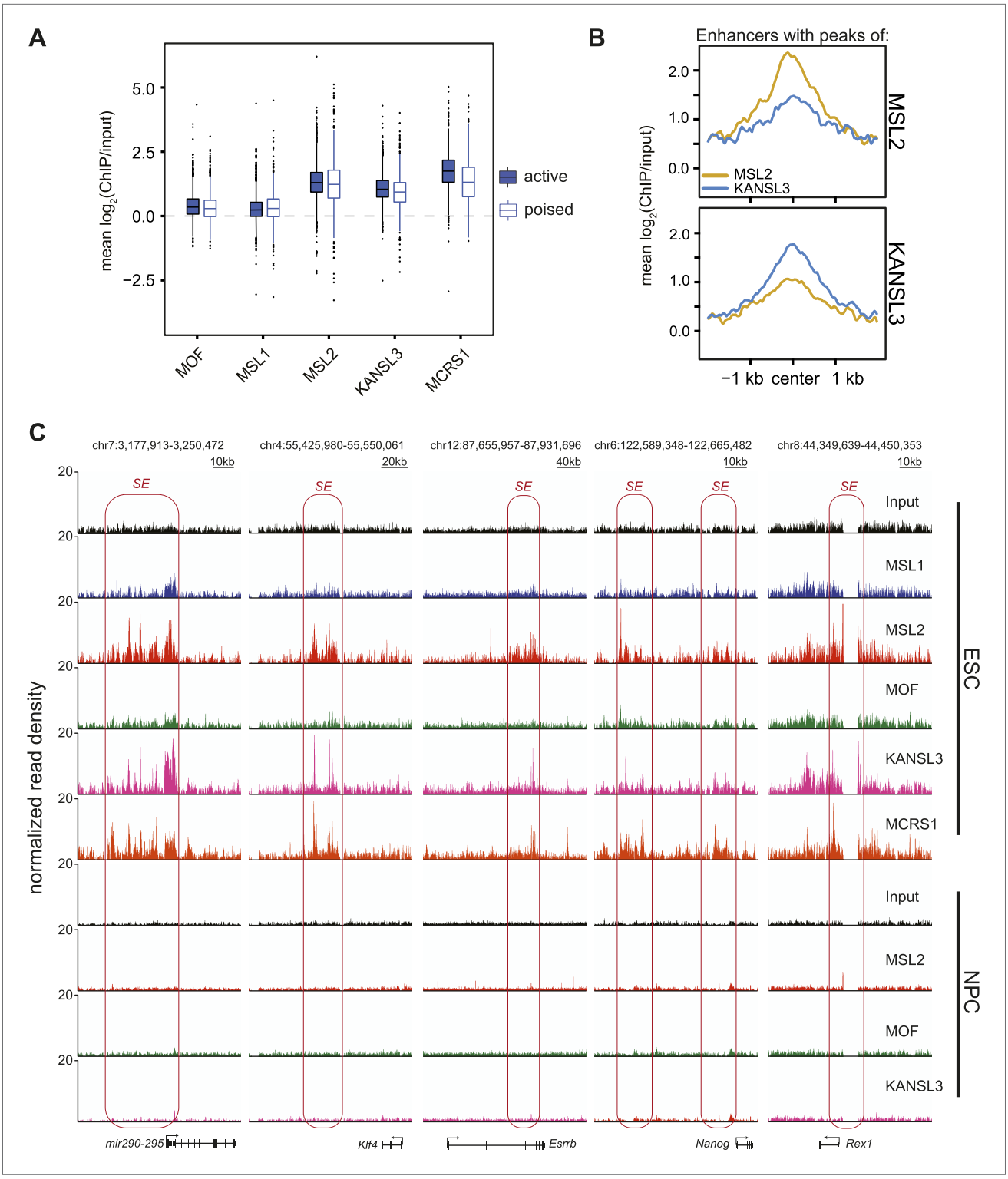

Figure 4—figure supplement 1. MSL2 and KANSL3 show strong enrichments at typical and super enhancers in ESCs.

DOI: 10.7554/eLife.02024.014

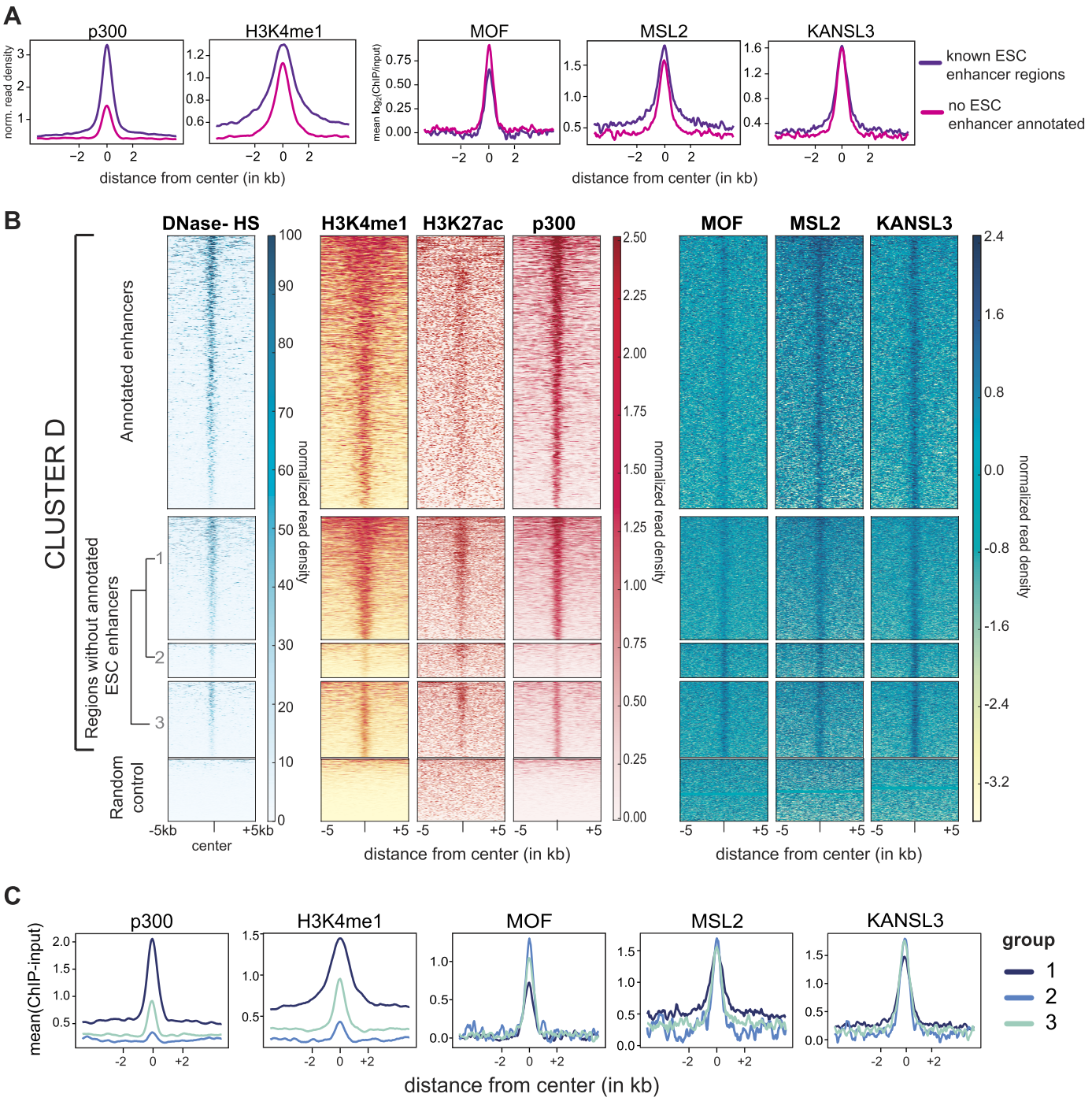

Figure 4—figure supplement 2. MOF is moderately enriched at non-canonical enhancers.
DOI: 10.7554/eLife.02024.015

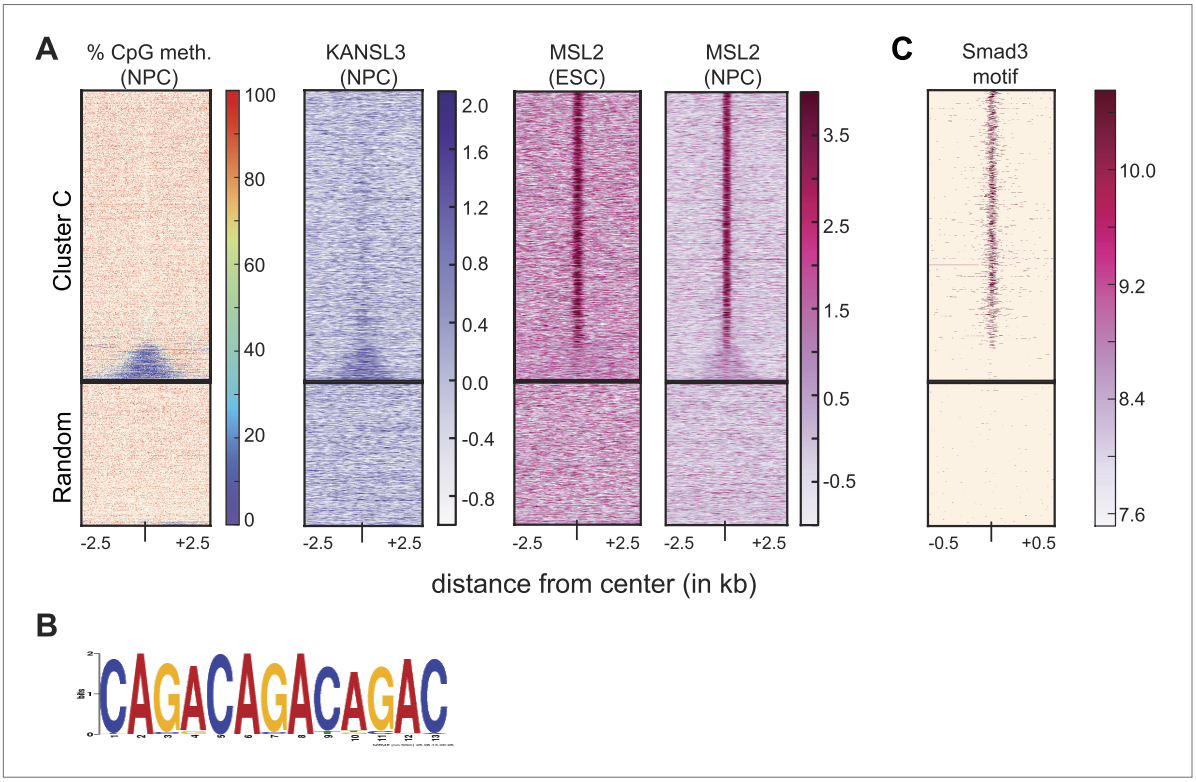

Figure 4—figure supplement 3. MSL2 has intergenic binding sites in DNA-hypomethylated regions that are enriched for SMAD3 binding sites.

DOI: 10.7554/eLife.02024.016

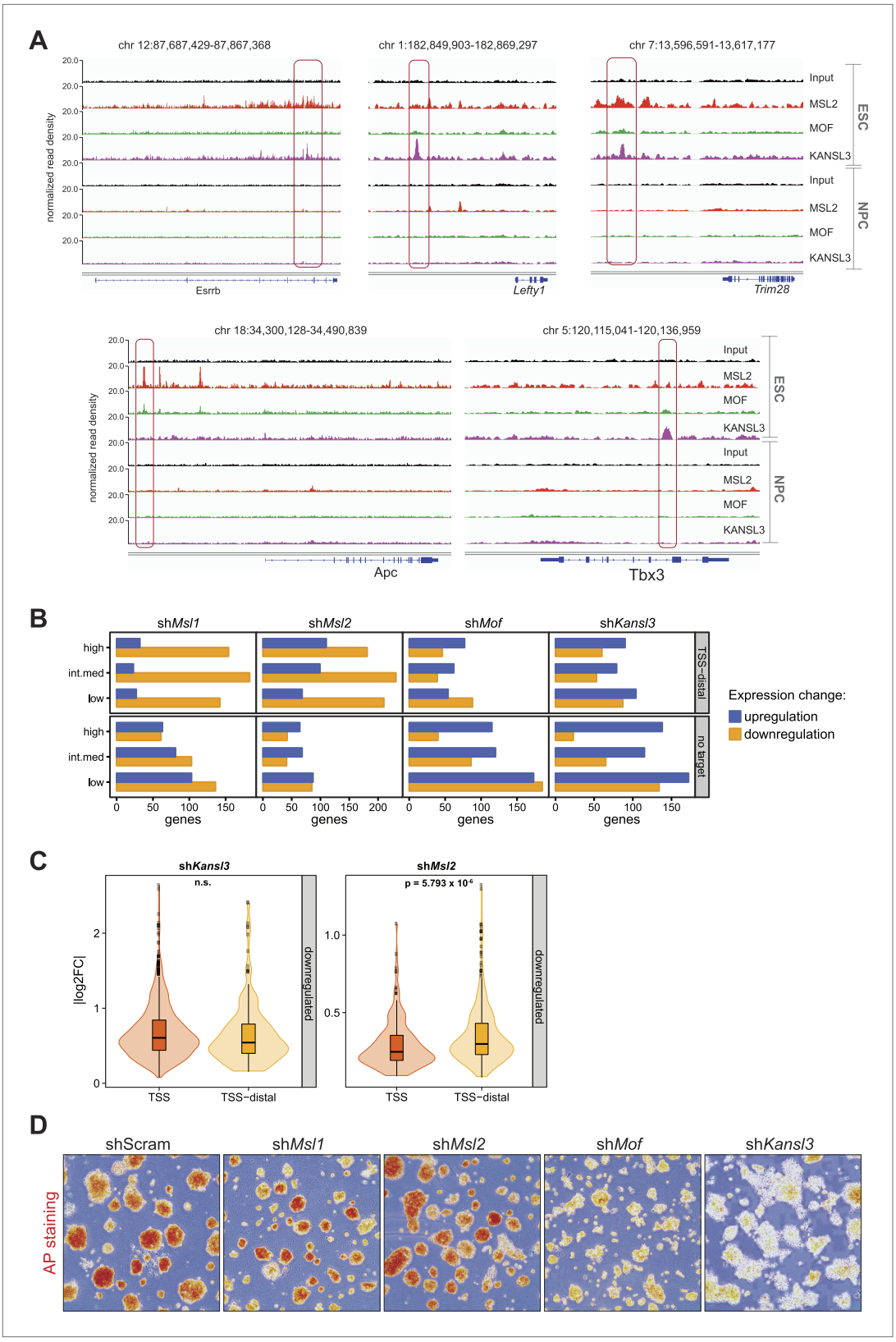

Figure 4—figure supplement 4. Biological significance of the TSS-distal binding sites of the investigated proteins.
DOI: 10.7554/eLife.02024.017

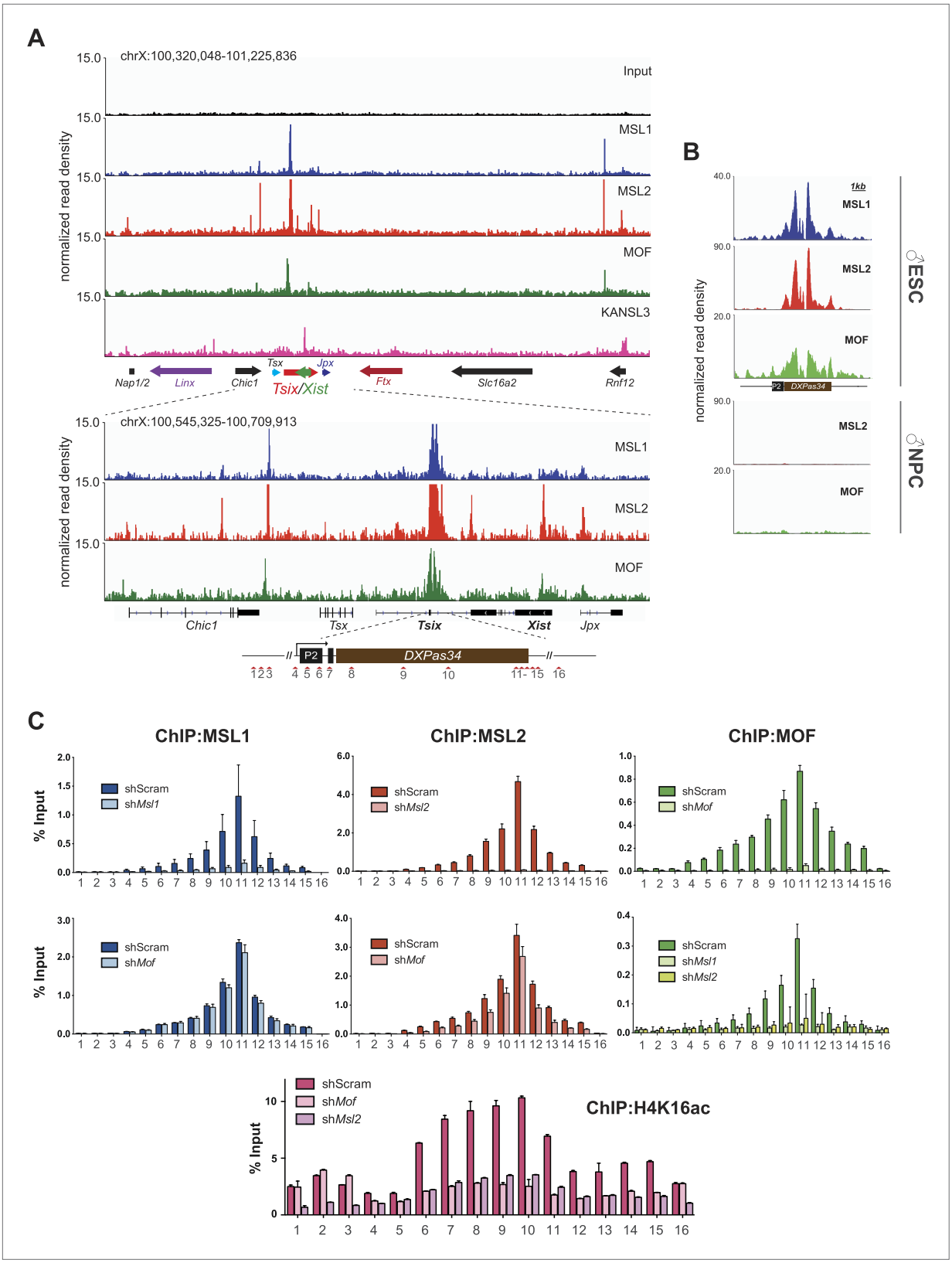

Figure 5. The MSL complex binds multiple loci within the X inactivation center including the *Tsix DXPas34* minisatellite enhancer. (**A**) Genome browser snapshots of the mouse X inactivation center (approximately 0.9 Mb) (upper panel) plus enlargement of the 164 kb region between *Chic1* and *Jpx/Enox* (lower panel). The signals shown are the sequencing-depth normalized profiles for ChIP-seq from ESCs (for corresponding profiles in NPCs see

Figure 5. Continued on next page

Figure 5. Continued

Figure 5—figure supplement 1A); colored arrows indicate genes of lncRNAs. The schematic representation of the *DXPas34* locus depicts the locations of the primer pairs that were used for ChIP-qPCR analyses (***Supplementary file 3B***). (**B**) Genome browser snapshots of the *DXPas34* minisatellite of sequencing-depth normalized ChIP-seq profiles in ESCs and NPCs. (**C**) ChIP-qPCR analyses of MSL1 (blue), MSL2 (red), MOF (green), and H4K16 acetylation (purple) across the *Tsix* major promoter (*P2*) and the *DXPas34* enhancer in male ESCs treated with the indicated shRNAs. For corresponding ChIP-qPCR in female ESCs see ***Figure 5—figure supplement 1C***. Panels in the middle show the effects of MOF depletion on the recruitment of MSL1 and MSL2 to *DXPas34* and vice versa. The bottom panel shows effects of depletion of control (dark pink), MOF (light pink) and MSL2 (purple) on the H4K16 acetylation signal. The labels of the x axes correspond to the arrowheads in (**A**). Results are expressed as mean ± SD of three biological replicates; cells were harvested on day 4 (*Msl1*, *Msl2*) or 5 (*Mof*) after shRNA treatment. For primer pairs see ***Supplementary file 3C***.

DOI: 10.7554/eLife.02024.018

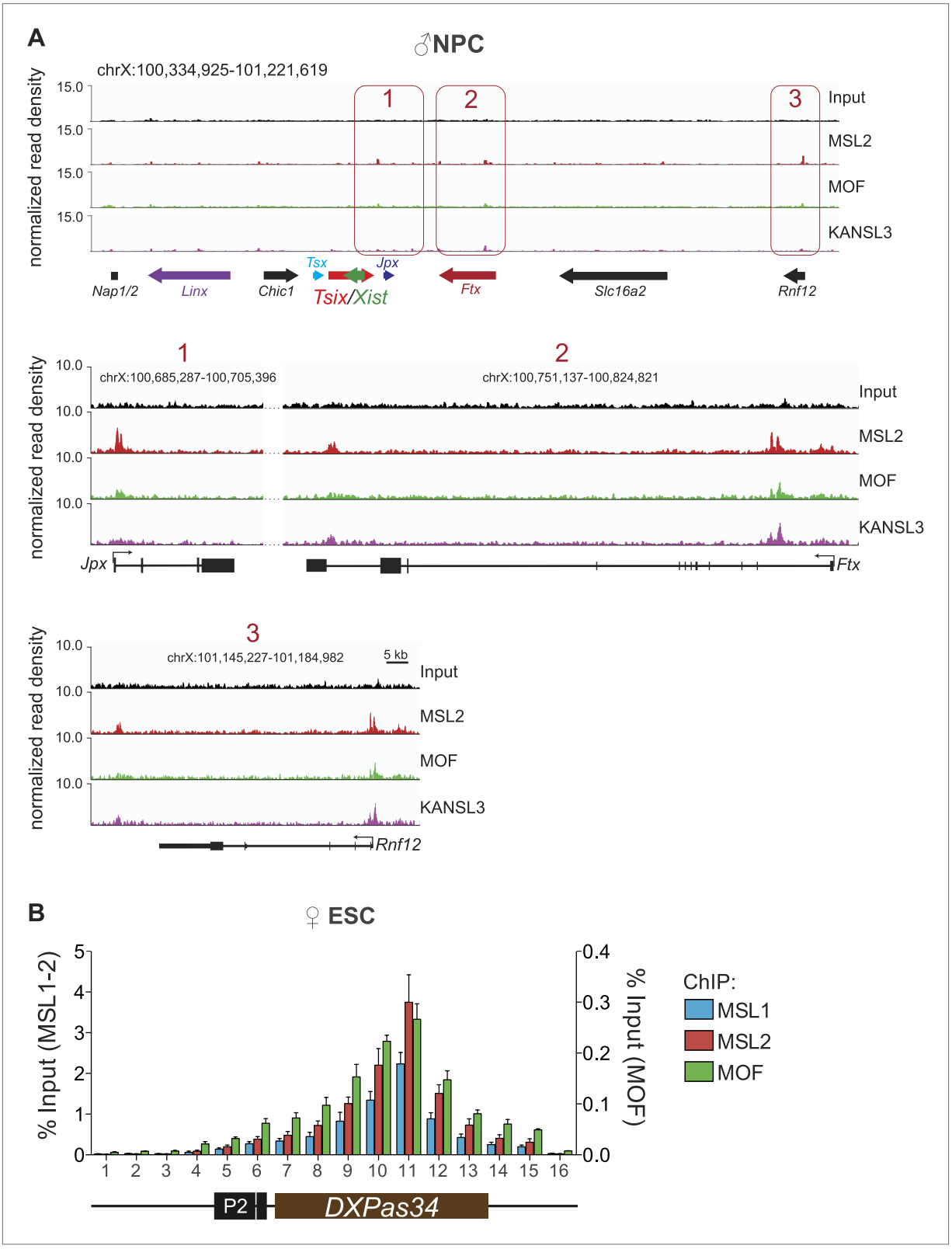

Figure 5—figure supplement 1. The MSL proteins bind to multiple loci within the X inactivation center (XIC).

DOI: 10.7554/eLife.02024.019

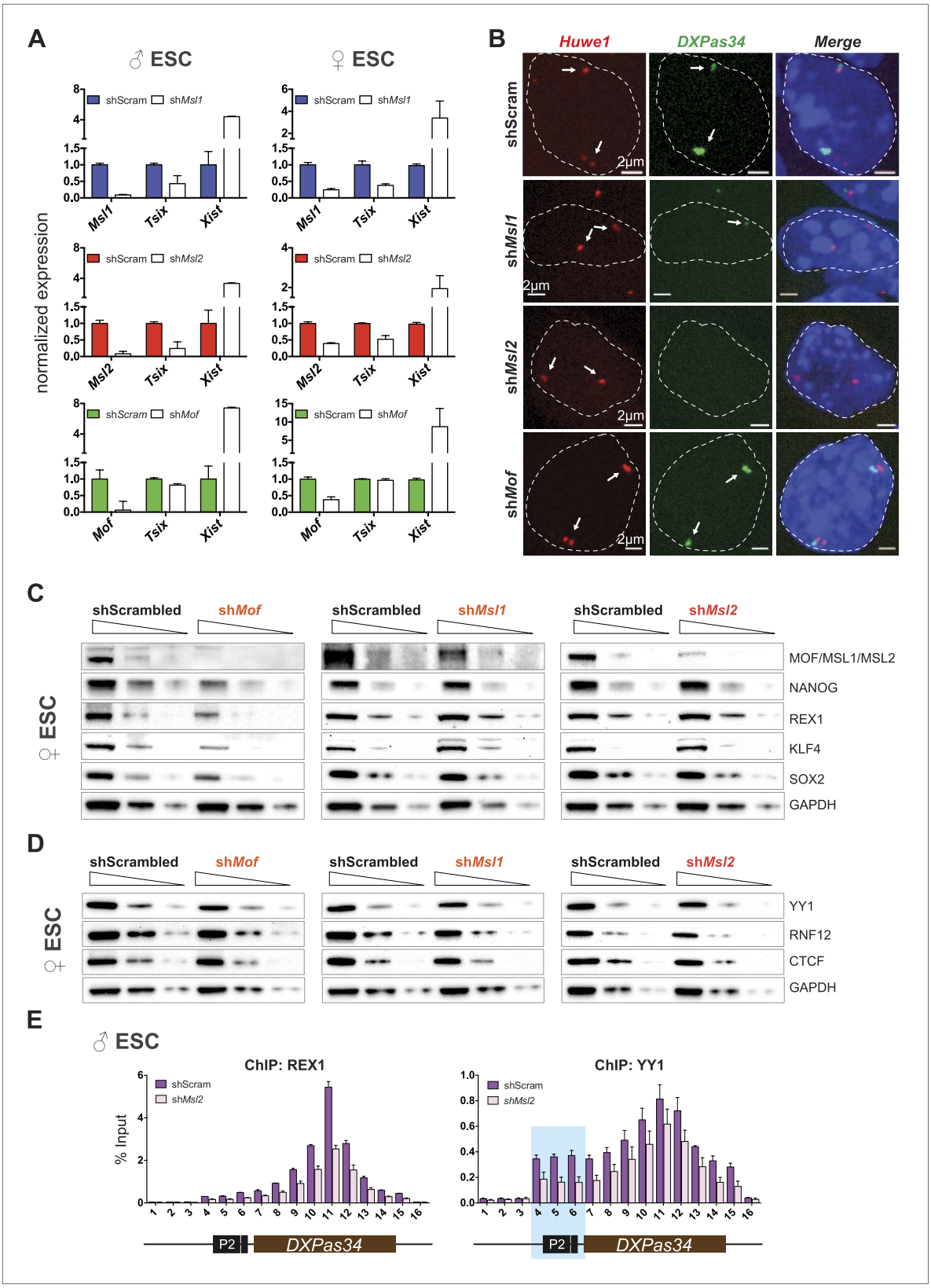

Figure 6. Depletion of MSL1 and MSL2 leads to downregulation of *Tsix* with concomitant upregulation of *Xist*. (**A**) Gene expression analysis for the indicated genes in male and female ESCs treated with scrambled RNA (shScram) or shRNA against *Msl1*, *Msl2*, or *Mof*. All results are represented as relative values normalized to expression levels in shScram (normalized to *Hprt*) and expressed as means ± SD in three biological replicates. (**B**) RNA-FISH

Figure 6. Continued on next page

Figure 6. Continued

for *Huwe1* (red) and *DXPas34* (green) in: scrambled control, sh*Msl1*-, sh*Msl2*-, and sh*Mof*-treated female ESCs. Nuclei were counterstained with DAPI (blue). White arrows denote foci corresponding to *Huwe1* or *Tsix*; dashed lines indicate nuclei borders. For additional images, phenotypes and quantifications see ***Figure 6—figure supplement 1A–C***. For probe references see 'Materials and methods'. (**C**) Western blot analyses of the pluripotency factors in scrambled-, *Mof*-, *Msl1*-, and *Msl2*-shRNA-treated female ESCs. For corresponding expression analyses see ***Figure 6—figure supplement 1D,E***. The respective dilution (100%, 30%, 10%) of loaded RIPA extracts is shown above each panel. GAPDH was used as the loading control. For antibodies see 'Materials and methods'. (**D**) Western blot analyses of the transcription factors involved in regulation of the XIC in scrambled-, *Mof*-, *Msl1*-, and *Msl2*-shRNA-treated female ESCs. The respective dilution (100%, 30%, 10%) of loaded RIPA extracts is shown above each panel. GAPDH was used as the loading control. (**E**) ChIP-qPCR analysis of REX1 (left panel) and YY1 (right panel) across the *Tsix* major promoter (P2) and *DXPas34* in male ESCs treated with the indicated shRNAs. The labels of the x axes correspond to the arrowheads in ***Figure 5A***. For all ChIP experiments, three biological replicates were used; results are expressed as mean ± SD; cells were harvested on day 4 (*Msl2*) or 5 (*Mof*) after shRNA treatment.

DOI: 10.7554/eLife.02024.020

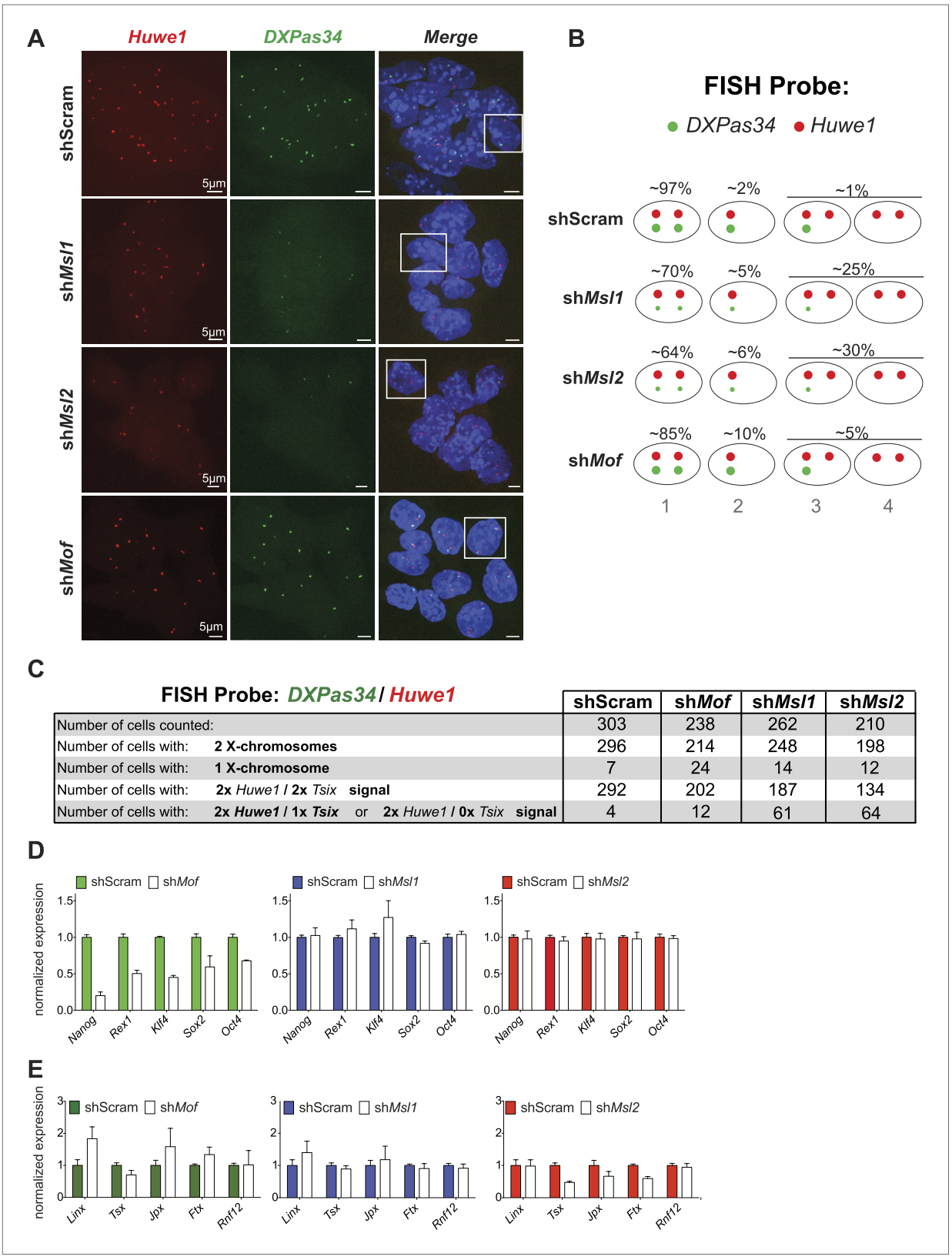

	shScram	sh*Mof*	sh*Msl1*	sh*Msl2*
Number of cells counted:	303	238	262	210
Number of cells with: **2 X-chromosomes**	296	214	248	198
Number of cells with: **1 X-chromosome**	7	24	14	12
Number of cells with: **2x** *Huwe1* / **2x** *Tsix* **signal**	292	202	187	134
Number of cells with: **2x *Huwe1* / 1x *Tsix*** or **2x** *Huwe1* / **0x** *Tsix* **signal**	4	12	61	64

Figure 6—figure supplement 1. Cells depleted of MSL1 or MSL2, but not MOF show loss of *DXPas34* foci.

DOI: 10.7554/eLife.02024.021

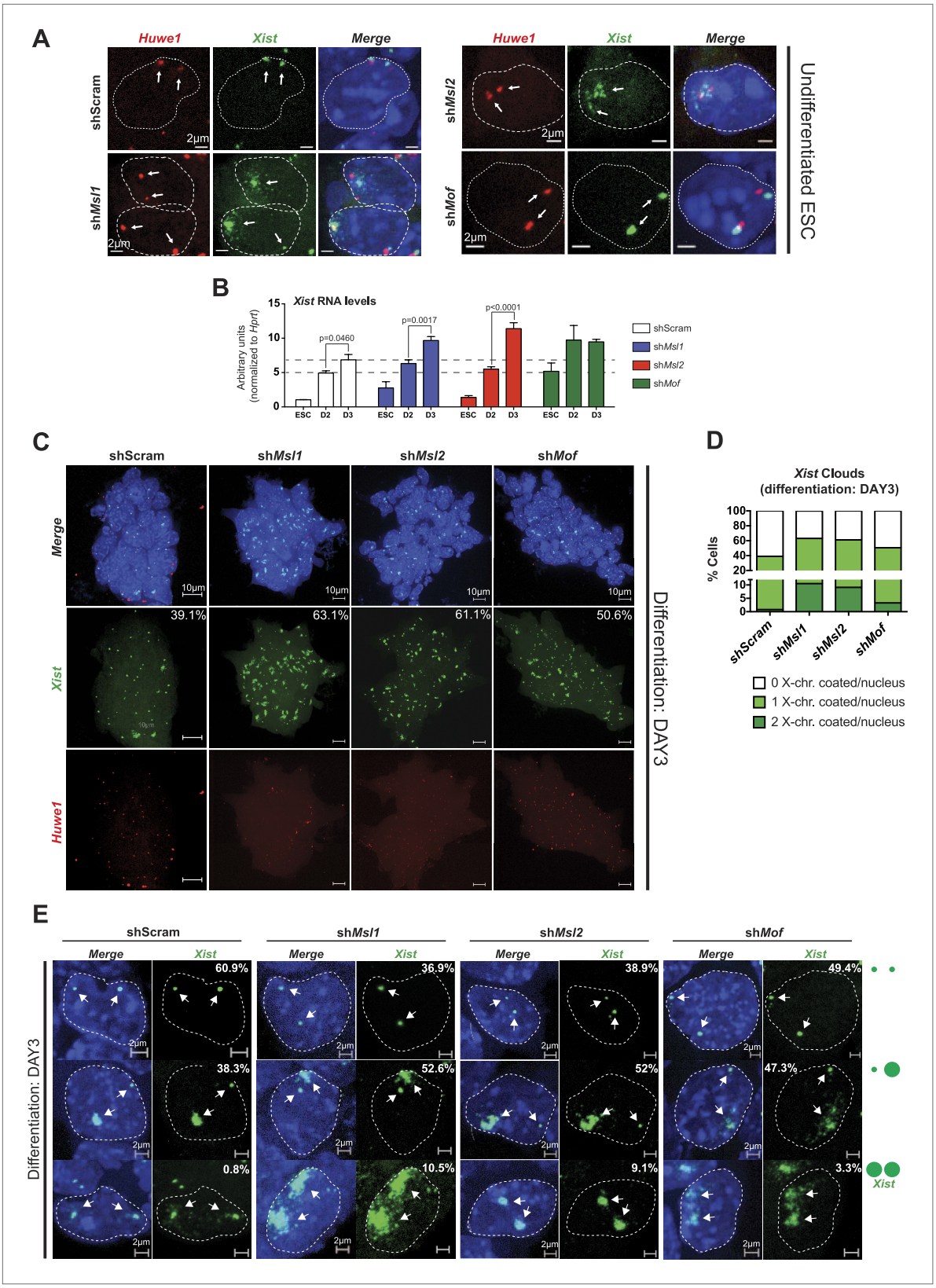

Figure 7. MSL1 and MSL2 depletion leads to enhanced and chaotic *Xist* accumulation in early differentiation. (**A**) RNA-FISH for *Huwe1* (red) and *Xist* (green) in: scrambled control, sh*Msl1*-, sh*Msl2*-, and sh*Mof*-treated female ESCs. Nuclei were counterstained with DAPI (blue). White arrows denote foci corresponding to *Huwe1* or *Xist*; dashed lines indicate nuclei borders. For additional images, phenotypes and quantifications see ***Figure 7—figure supplement 1B–D***.

Figure 7. Continued on next page

Figure 7. Continued

For probe references see 'Materials and methods'. (**B**) Expression analysis for *Xist* in undifferentiated, day 2 (D2) and day 3 (D3) differentiating female ESCs treated with scrambled RNA (shScram) or shRNA against *Mof*, *Msl1*, and *Msl2*. All results are represented as arbitrary units (*Xist* expression in undifferentiated ESCs = 1) normalized to expression levels in shScram (normalized to *Hprt*) and expressed as means ± SD in three biological replicates. p-values for D2-to-D3 expression change were obtained using unpaired *t* test. (**C**) RNA-FISH for *Huwe1* (red) and *Xist* (green) in: scrambled control, sh*Msl1*-, sh*Msl2*-, and sh*Mof*-treated differentiating female ESCs. Nuclei were counterstained with DAPI (blue). RNA-FISH was performed on the sixth day of knockdown (after 72 hr of differentiation). Percentages indicate number of cells with at least one *Xist* cloud for each of the knockdowns. For additional images of multicellular colonies see ***Figure 7—figure supplement 2A***. (**D**) Bar plot summarizing the percentage of *Xist* clouds for individual knockdowns in differentiating (DAY3) female ESCs for individual knockdowns. Cells were divided into three categories: cells carrying no *Xist* clouds (white), single *Xist* cloud (light green), or two *Xist* clouds (dark green). For quantifications, see ***Figure 7—figure supplement 2B***. (**E**) RNA-FISH for *Xist* (green) in: scrambled control, sh*Msl1*-, sh*Msl2*-, and sh*Mof*-treated differentiating (DAY3) female ESCs. Here, we show examples of individual nuclei carrying different patterns of *Xist* accumulation. Percentages correspond to the frequency of the shown *Xist* pattern within the population of cells. White arrows denote *Xist* foci; dashed lines indicate nuclei borders. For quantifications see ***Figure 7—figure supplement 2B***.

DOI: 10.7554/eLife.02024.022

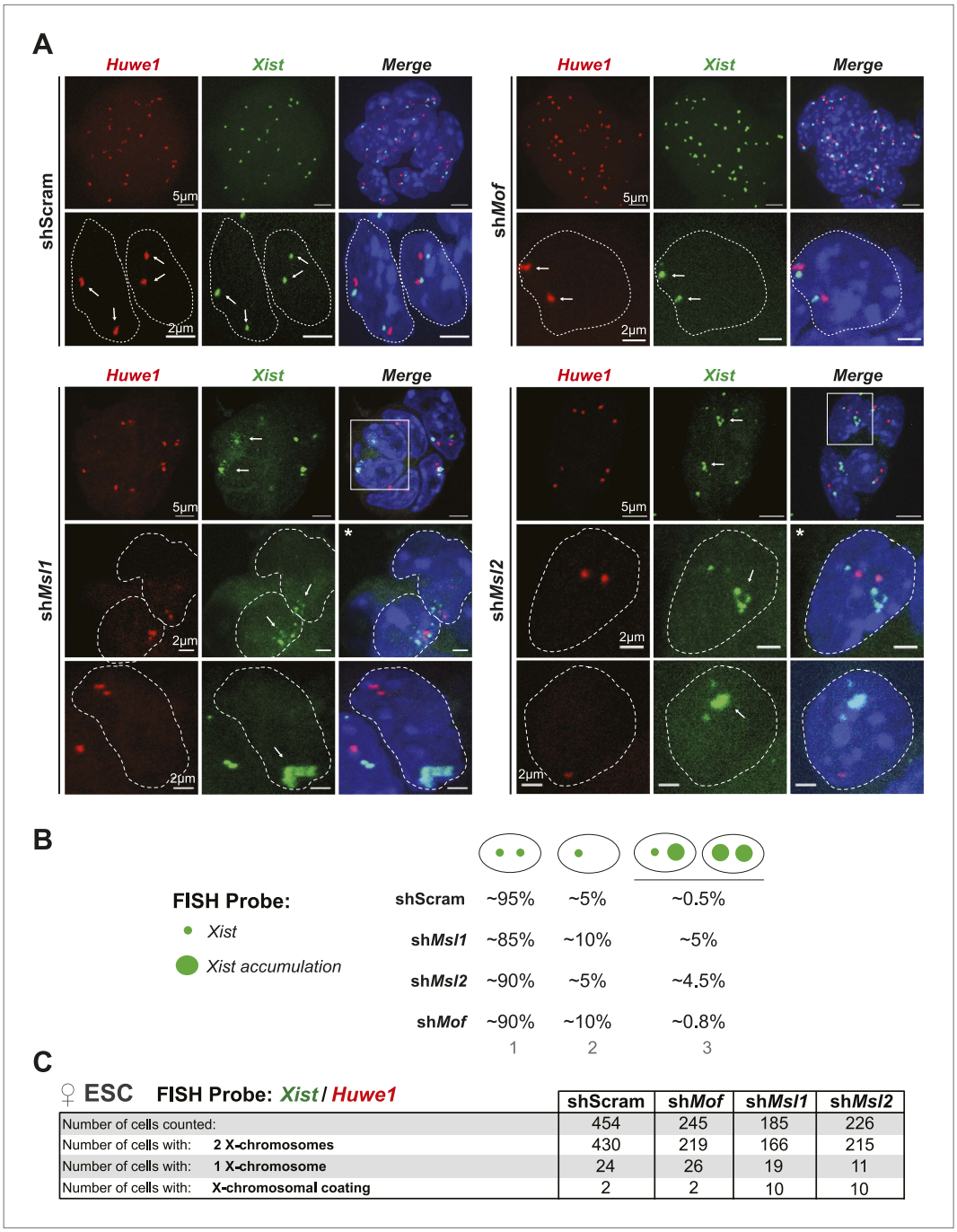

	shScram	sh*Mof*	sh*Msl1*	sh*Msl2*
Number of cells counted:	454	245	185	226
Number of cells with: **2 X-chromosomes**	430	219	166	215
Number of cells with: **1 X-chromosome**	24	26	19	11
Number of cells with: **X-chromosomal coating**	2	2	10	10

Figure 7—figure supplement 1. Depletion of MSL1 and MSL2 leads to occasional accumulation and spreading of *Xist* in undifferentiated ESCs.

DOI: 10.7554/eLife.02024.023

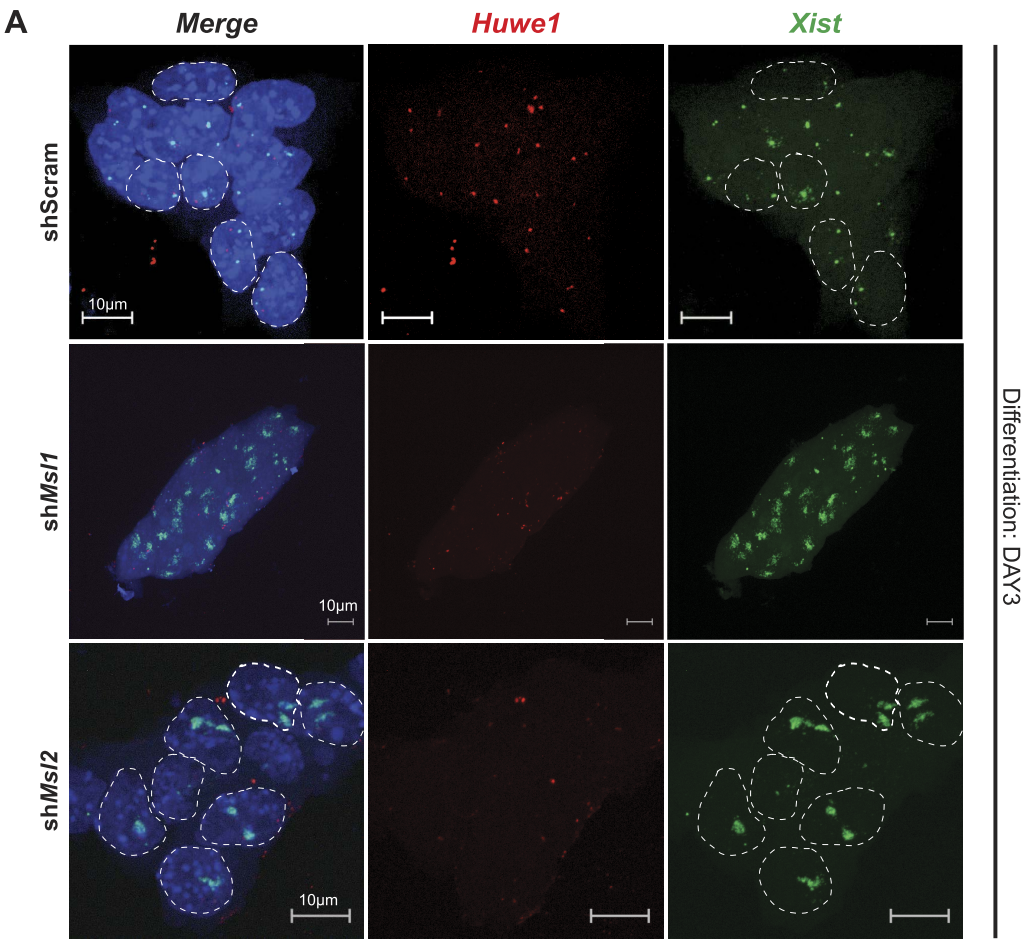

B

FISH Probe: *Xist* / *Huwe1*	shScram	sh*Msl1*	sh*Msl2*	sh*Mof*
Number of cells counted:	253	209	285	239
Number of cells with: **0 *Xist* Clouds**	154 (60.9%)	77 (36.9%)	111 (38.9%)	118 (49.4%)
Number of cells with: **1 *Xist* Cloud**	97 (38.3%)	110 (52.6%)	148 (52%)	113 (47.3%)
Number of cells with: **2 *Xsit* Clouds**	2 (0.8%)	22 (10.5%)	26 (9.1%)	8 (3.3%)

Figure 7—figure supplement 2. Depletion of MSL1 and MSL2 lead to enhanced *Xist* accumulation in differentiating ESCs.

DOI: 10.7554/eLife.02024.024

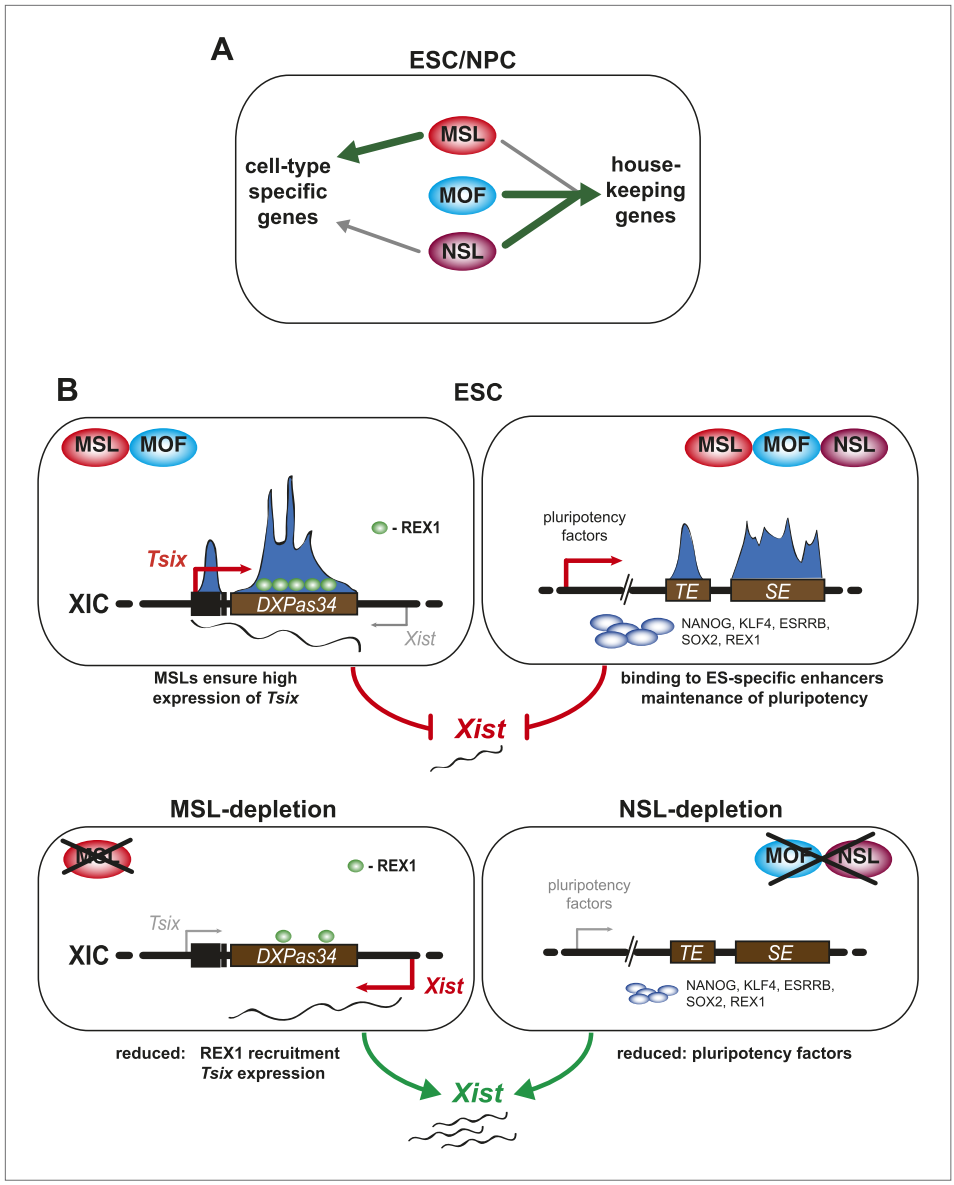

Figure 8. A summary model. Shared and distinct pathways by which MOF, MSLs and NSLs regulate gene expression, pluripotency, and the X inactivation center. (**A**) In this study, we have identified several modes of concurrent and independent binding of mammalian MOF, MSL and NSL proteins. We find that all complexes bind to promoters of housekeeping genes in ESCs and NPCs with NSL complex members occupying the majority of the target genes, while MOF and MSL proteins bind NSL-bound genes in a more restricted manner. Furthermore, we observe that upon differentiation, KANSL3 and MSL2 additionally occupy TSSs of different sets of cell-type-specific genes in the absence of MOF. (**B**) When we studied the functions of MSL and NSL complexes at the murine X inactivation center, we determined two basic mechanisms by which the different proteins affect the maintenance of two active X chromosomes in ESCs. (1) MSLs bind to the promoter and enhancer of *Tsix* whose transcription represses *Xist* expression. Upon depletion of MSLs, *Tsix* expression is compromised, so is REX1 recruitment to the *Tsix* locus. Consequently, *Xist* is increasingly transcribed and can occasionally accumulate. (2) In addition, MOF, MSLs, and NSLs bind to typical enhancers (TE) and super enhancers (SE) in ESCs, and notably those of pluripotency factors. In WT ESCs, the high expression of pluripotency factors is another layer of *Xist* repression. The depletions of MOF or KANSL3, but not of MSL1 or MSL2 reduce the expression of pluripotency factors involved in *Xist* repression causing a *Tsix*-independent increase of *Xist* expression.
DOI: 10.7554/eLife.02024.025